Materials Horizons

Experimental Validation of High Thermoelectric Performance in *RE*CuZnP_2 Predicted by High-Throughput DFT Calculations

Journal:	*Materials Horizons*
Manuscript ID	MH-COM-07-2020-001112.R1
Article Type:	Communication
Date Submitted by the Author:	17-Sep-2020

Complete List of Authors:	Pöhls, Jan-Hendrik; University of Alberta, Department of Chemistry; McGill University, Physics Chanakian, Sevan; Michigan State University Park, Junsoo; Lawrence Berkeley National Laboratory, Energy Storage & Distributed Resources Division Ganose, Alex; Lawrence Berkeley National Laboratory Dunn, Alexander; Lawrence Berkeley National Lab, Energy & Environmental Technologies Division Friesen, Nick; University of Alberta, Chemistry Bhattacharya, Amit; University of Alberta, Department of Chemistry Hogan, Brea; University of California Los Angeles Bux, Sabah; Jet Propulsion Laboratory, Jain, Anubhav; Lawrence Berkeley National Lab, Energy & Environmental Technologies Division Mar, Arthur; University of Alberta, Zevalkink, Alexandra; Michigan State University, Chemical engineering and materials science

New Concepts Statement

This investigation of *RE*$CuZnP_2$ (*RE* = rare earth) is the *first* in-depth study of transport properties in *quaternary* $CaAl_2Si_2$-type compounds, a promising class of thermoelectric materials. This study demonstrates that the combined application of DFT calculations with advanced physics-based scattering calculations delivers new insight on the underlying mechanisms of thermoelectric transport. The results directly challenge the usual assumption that acoustic phonon scattering is the limiting factor of electron transport in most thermoelectric materials; instead, polar optical phonon scattering is likely more important than previously believed. Moreover, the calculations shed light on the unexpectedly low lattice thermal conductivity in *RE*$CuZnP_2$: despite high bulk moduli and speeds of sound, strongly anharmonic bonding can significantly reduce the thermal conductivity. These insights on the mechanisms of electron and heat transport have broader implications to the materials science community, by guiding researchers to discover more efficient thermoelectric materials in applying new concepts to optimize their properties. The low computational cost of these methods could also herald an exciting era of DFT-guided materials discovery.

COMMUNICATION

Experimental Validation of High Thermoelectric Performance in *RE*CuZnP$_2$ Predicted by High-Throughput DFT Calculations

Received 00th January 20xx,
Accepted 00th January 20xx

DOI: 10.1039/x0xx00000x

Jan-Hendrik Pöhls,[a,b] Sevan Chanakian,[c†] Junsoo Park,[d] Alex M. Ganose,[d] Alexander Dunn,[d] Nick Friesen,[a] Amit Bhattacharya,[a] Brea Hogan,[e] Sabah Bux,[e] Anubhav Jain,[d] Arthur Mar,[a¥] and Alexandra Zevalkink[c*]

Accurate density functional theory calculations of the interrelated properties of thermoelectric materials entail high computational cost, especially as crystal structures increase in complexity and size. New methods involving ab initio scattering and transport (AMSET) and compressive sensing lattice dynamics are used to compute the transport properties of quaternary $CaAl_2Si_2$-type rare-earth phosphides *RE*CuZnP$_2$ (*RE* = Pr, Nd, Er), which were identified to be promising thermoelectrics from high-throughput screening of 20,000 disordered compounds. Experimental measurements of the transport properties agree well with the computed values. Compounds with stiff bulk moduli (>80 GPa) and high speeds of sound (>3,500 m s^{-1}) such as *RE*CuZnP$_2$ are typically dismissed as thermoelectric materials because they are expected to exhibit high lattice thermal conductivity. However, *RE*CuZnP$_2$ exhibits not only low electrical resistivity, but also low lattice thermal conductivity (~1 W m^{-1} K^{-1}). Contrary to prior assumptions, polar optical phonon scattering was demonstrated to be the primary mechanism limiting the electronic mobility of these compounds, raising questions about existing assumptions of scattering mechanisms in this class of thermoelectric materials. The resulting thermoelectric performance (*zT* of 0.5 for ErCuZnP$_2$ at 800 K) is among the best observed in phosphides and can likely be improved with further optimization.

Introduction

More than half of the world's energy produced by non-renewable sources is wasted as a non-usable form of thermal energy. Part of the lost useful energy could be recovered by converting heat into electrical energy using thermoelectric materials. However, the high costs and low efficiencies of commercial thermoelectric materials limit affordable applications. The efficiency is proportional to the thermoelectric figure of merit, $zT = S^2T/(\rho\kappa)$, which depends on the Seebeck coefficient S, the electrical resistivity ρ, the thermal conductivity κ (having electronic, κ_{el}, and phononic, κ_{ph}, contributions) and the absolute temperature T.[1] Optimizing thermoelectric efficiency is a complicated balancing act because the factors are dependent of each other.

The search for high-performance thermoelectric materials can be accelerated by high-throughput screening of candidates evaluated by density functional theory (DFT) calculations.[2-8] Based on ongoing screening of the electrical properties (viz., power factor, $PF=S^2/\rho$) for over 20,000 disordered inorganic compounds taken from the Inorganic Crystal Structure Database (ICSD),[9] the phosphides *RE*CuZnP$_2$ (*RE* = trivalent rare-earth metal) have emerged as promising candidates. These compounds are quaternary derivatives of a family of AM_2X_2 compounds that adopt the trigonal $CaAl_2Si_2$-type structure and exhibit electrical and thermal properties suitable for thermoelectric materials (e.g., Mg_3Sb_2,[10-12] $EuCd_2Sb_2$[13]). Despite restrictions on the formation of these AM_2X_2 compounds (requiring a valence electron count of 16 and a d^0, d^5, or d^{10} configuration for *M*), they are numerous and diverse. The *A* cation is commonly divalent but can be monovalent or trivalent with appropriate substitution of the other components to maintain the electron count, as exemplified by *RE*CuZnP$_2$, which contains Cu^+ and Zn^{2+} mixed on the *M* site (Figure S3, Supporting Information).[14-16]

In general, semiconducting compounds containing light atoms such as C, N, or P often exhibit excellent electrical properties,[17] but they would be expected to have stiff bonds, leading to high thermal conductivities. However, some metal phosphides have been predicted to show low lattice thermal conductivities,[18-20] suggesting that lightweight compounds should not be dismissed so easily. The transport properties of many $CaAl_2Si_2$-type compounds remain largely uninvestigated, especially of nitride and phosphide members,[21-28] as well as those containing a trivalent *A* cation. Given that site disorder

[a.] *Department of Chemistry, University of Alberta, Edmonton, AB T6G 2G2, Canada*
[b.] *Department of Physics, McGill University, Montreal, QC H3A 2T8, Canada*
[c.] *Department of Chemical Engineering and Materials Science, Michigan State University, East Lansing, MI 48824, USA*
[d.] *Energy Technologies Area, Lawrence Berkeley National Laboratory, Berkeley, CA 94720, USA*
[e.] *Thermal Energy Conversion Research and Advancement Group, Jet Propulsion Laboratory, California Institute of Technology, Pasadena, CA 91109, USA*
† J.-H. Pöhls and S. Chanakian contributed equally to this work.
¥ E-mail: arthur.mar@ualberta.ca
** E-mail: alexzev@msu.edu*
Electronic Supplementary Information (ESI) available: SeeDOI: 10.1039/x0xx00000x

would also lower thermal conductivity, we hypothesize that the phosphides *RE*CuZnP$_2$ are attractive candidates for thermoelectric materials.

To test this hypothesis and to validate the predictions from the computational screening, three *RE*CuZnP$_2$ (*RE* = Pr, Nd, Er) compounds were synthesized and their thermoelectric properties were measured. These experimental results were compared with first-principles calculations of electron and phonon transport properties to gain insight on the scattering mechanisms that determine thermoelectric performance.[29,30] In particular, starting solely from first-principles input, the *ab initio* scattering and transport (AMSET) software package was used to compute carrier lifetimes arising from acoustic deformation potential (ADP), polar-optical phonon (POP), and ionized impurity (IMP) scattering processes. In a recent study[31], AMSET was applied to 16 simple semiconductors and demonstrated excellent agreement against both experimental measurements on single crystals and state-of-the-art calculations (Electron-Phonon Wannier, EPW) of electronic mobility and Seebeck coefficient. However, unlike other methods whose computational expense limits their use to small highly-symmetric systems, AMSET can be applied to complex compounds (including disordered ones such as *RE*CuZnP$_2$) and in a high-throughput manner, enabling information about scattering to be extracted for a wide variety of materials. We evaluate how well this new computational approach agrees with the experimental results on *RE*CuZnP$_2$ and whether other related phosphides may be feasible thermoelectric materials.

Results and Discussion

Synthesis

Samples of *RE*CuZnP$_2$ (*RE* = Pr, Nd, Er) were prepared by high-temperature reactions of the elements. Powder X-ray diffraction (XRD) confirmed that they crystallize in the $CaAl_2Si_2$-type structure [space group $P\bar{3}m1$ (no. 164)] (Figure S1), with lattice parameters that agree with those reported previously (Table S1).[14] They were densified into pressed pellets by spark plasma sintering for property measurements.

Elastic Properties

The intrinsic lattice thermal conductivity of a material depends on its elastic properties, which were calculated and measured for *RE*CuZnP$_2$ compounds (Table 1).[32] On progressing from the Pr to the Er member, the stiffness increases slightly (as gauged by the bulk, Young's, and shear modulus), consistent with smaller lattice parameters and shorter bond lengths,[14] but the Poisson ratio does not change significantly. For PrCuZnP$_2$ and ErCuZnP$_2$, the average speed of sound, $v_{avg} = (v_L+2v_T)/3$, is about 3650 m s^{-1}, which is higher than typically found in other $CaAl_2Si_2$-type compounds (e.g., Mg_3Sb_2, 2800 m s^{-1}; $EuZn_2Sb_2$, 2400 m s^{-1});[33] to date, only $CaMg_2Sb_2$ has a comparable value of 3200 m s^{-1}.[34] In general, the thermoelectric properties of stiffer $CaAl_2Si_2$-type compounds, namely phosphides and arsenides, are not as well studied as the antimonide members.[26,35,36] Filling this gap will help clarify the relationship between bonding and properties in these compounds.

Table 1. Experimental and computed elastic properties [bulk modulus (*B*), Young's modulus (*E*), shear modulus (*G*), Poisson ratio (ν); longitudinal (v_L) and transverse speed of sound (v_T)] for *RE*CuZnP$_2$ compounds. Note: NdCuZnP$_2$ was not measured due to geometric restrictions.

Compound	*B* [GPa]	*E* [GPa]	*G* [GPa]	ν	v_L [m s^{-1}]	v_T [m s^{-1}]
PrCuZnP$_2$ (exp.)	87	126	50	0.26	5,170	2,940
PrCuZnP$_2$ (comp.)	87	142	58	0.23	5,340	3,180
NdCuZnP$_2$ (comp.)	88	143	58	0.23	5,300	3,140
ErCuZnP$_2$ (exp.)	95	142	57	0.25	5,080	2,910
ErCuZnP$_2$ (comp.)	94	147	59	0.24	5,080	2,970

Electrical Transport Properties

The electrical resistivity (ρ), Hall mobility (μ_H), Hall carrier concentration (n_H), and Seebeck coefficient (*S*) of *RE*CuZnP$_2$ compounds were measured experimentally as a function of temperature and compared with calculated results (Figure 1).

For all samples, the resistivity increases with higher temperature and the carrier concentration is >10^{19} cm^{-3} (Figure 1 (a) and 1 (c)), implying that these compounds are highly degenerate *p*-type semiconductors. Substitution with a heavier *RE* component (from Pr to Er) lowers the resistivity by an order of magnitude, due primarily to an increase in carrier concentration in ErCuZnP$_2$ relative to the two other compounds. The higher carrier concentration could be the result of sample processing or suggest that cation vacancies have a lower formation energy in ErCuZnP$_2$.[37]

The hole mobility is relatively low for *RE*CuZnP$_2$ samples, ranging from 37 to 50 cm^2 V^{-1} s^{-1} at 300 K on progressing from *RE* = Pr to Er (Figure 1 (b)), compared to other rare-earth-containing compounds with the $CaAl_2Si_2$-type structure (e.g., $EuZn_2Sb_2$, 250 cm^2 V^{-1} s^{-1};[38] $YbZn_2Sb_2$, 130 cm^2 V^{-1} s^{-1};[39] $EuMg_2Bi_2$, 192 cm^2 V^{-1} s^{-1}).[40] The mobility reported previously in the related phosphide YbCuZnP$_2$ is even lower (11 cm^2 V^{-1} s^{-1} at 300 K).[26] Given that the mobility, $\mu = (e\cdot\tau_e)/m^*$, depends on the competing effects of effective mass m^* and relaxation time τ_e, first-principles calculations were carried out to gain insight on their roles. The electronic band structures, calculated using DFT with the Heyd–Scuseria–Ernzerhof (HSE06) exchange-correlation functional,[41] reveal that the *RE*CuZnP$_2$ compounds are small band gap semiconductors (E_g = 0.52 eV (Nd), 0.54 eV (Pr), 0.73 eV (Er)) with the valence band maximum at the Γ point (Figure S4). Note, experiments indicate that the materials are paramagnetic above room temperature (>0.3 K for ErCuZnP$_2$).[14] For each compound, the conductivity effective mass m_c^* was evaluated at the experimental carrier concentration and is the weighted average of three bands that nearly converge at the Γ point.[42] At 300 K, the value of m_c^* for ErCuZnP$_2$ (0.43 m_e) is larger than for NdCuZnP$_2$ (0.38 m_e) and PrCuZnP$_2$ (0.36 m_e). To check for contributions from bands below the band edge, m_c^* was also evaluated as a function of chemical potential;[43] ErCuZnP$_2$ retains the highest m_c^* regardless of chemical

potential. These values are similar to the only other report of m_c* for a $CaAl_2Si_2$-type compound, namely *p*-type Mg_3Sb_2 (0.34 m_e at a carrier concentration of 10^{19} cm^{-3}).[44]

To understand the scattering physics in more detail, it is of interest to calculate the transport properties, which requires electronic band structures as the primary input. Although existing methods to evaluate electron-phonon scattering such as Electron–Phonon Wannier (EPW)[45] can yield accurate scattering rates, they are not feasible for complex compounds due to their high computational cost. As the first application of AMSET[31] to examine new thermoelectric materials, scattering rates and carrier mobilities were calculated for *RE*$CuZnP_2$ using the momentum relaxation time approximation.[46] Three scattering mechanisms were considered: ionized impurities, acoustic deformation potential, and polar-optical phonons.

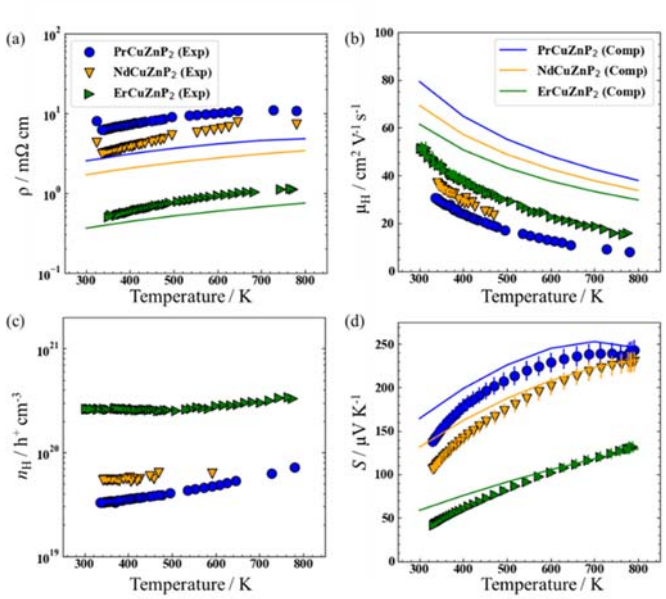

Figure 1. Experimental measurements (symbols) and AMSET computations (solid lines) of (a) electrical resistivity, (b) electrical mobility, (c) charge carrier concentrations, and (d) Seebeck coefficient of *RE*$CuZnP_2$ compounds. AMSET calculations use the temperature-average experimental carrier concentration.

The AMSET results were obtained at the experimental temperature-averaged Hall carrier concentrations. The mobilities are shown for all three compounds in Figure S5 and highlighted for $NdCuZnP_2$ in Figure 2. The chief mechanisms that are predicted to limit the mobilities are polar-optical phonon and, to a lesser extent, ionized impurity scattering. In contrast, acoustic deformation scattering is not predicted to affect the hole transport significantly, given the small absolute valence band deformation potentials (~1.4 eV) and stiff elastic constants (Table 1). This is rather surprising, because the experimental temperature dependence of the hole mobility (Figure S7) suggests that acoustic scattering is the dominant mechanism, as would be commonly assumed for thermoelectric materials used in mid-to-high temperature ranges.[47] In fact, acoustic scattering as a dominant mechanism is contradicted by many recent state-of-the-art computational studies, which indicate that polar-optical phonon scattering is the most important mechanism in many classes of high-performance heteropolar thermoelectric materials (e.g., SnSe, PbTe, half- and full-Heusler compounds),[48-51] as is the case here for *RE*$CuZnP_2$.

To confirm that the presence of f-electrons and disorder of the Cu/Zn site in *RE*$CuZnP_2$ do not engender unusual features, analogous AMSET calculations were carried out for the related simpler compound $CaZn_2P_2$. The results confirm that polar-optical phonon scattering also dominates in $CaZn_2P_2$ (Figure S6), suggesting that this mechanism is important in other $CaAl_2Si_2$-type compounds. $CaZn_2P_2$ is predicted to have a lower hole mobility than *RE*$CuZnP_2$ because of its higher m_c* (0.47 m_e at n = 10^{19} cm^{-3}) and smaller dielectric constants, leading to reduced electronic screening. The present AMSET results suggest that further understanding of the scattering mechanisms in $CaAl_2Si_2$-type compounds is required to develop concepts to improve their thermoelectric performance.

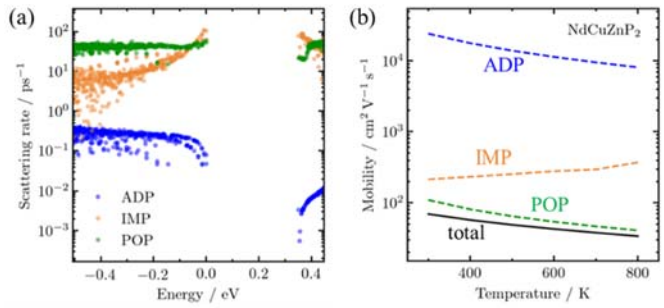

Figure 2. (a) Electron scattering rate and (b) temperature-dependent theoretical mobility of $NdCuZnP_2$ as calculated by AMSET are dominated by polar-optical phonon (POP) and ionized impurity (IMP) scattering while acoustic deformation potential (ADP) scattering plays an insignificant role.

Compared to the experimentally measured mobilities for *RE*$CuZnP_2$, the computed values are overestimated (Figure 1 (b)); however, the AMSET values should be considered as upper limits as the input DFT calculations were performed using completely ordered structures and boundary scattering, or other mesoscale imperfections not taken into account. The predicted trend in mobility as a function of *RE* substitution is opposite to that observed. However, the experimental mobility of the samples can be controlled by many factors (e.g., impurities, porosity, grain boundaries, pores, etc.), and may not reflect inherent differences in the electronic structure. In particular, the Er-containing samples have a larger grain size, as evidenced by the powder XRD patterns, which reveal narrower peaks compared to those for the Pr- and Nd-containing samples (Figure S2). The computed resistivities, evaluated at the temperature-averaged experimental Hall carrier concentrations, show reasonable agreement with the experimental values (Figure 1(a)), but they are somewhat underestimated, due to the overestimation of mobility.

The measured Seebeck coefficients of *RE*$CuZnP_2$ are positive, increase with higher temperature, and are inversely proportional to carrier concentration (Figure 1 (d)). For the Pr- and Nd-containing samples, saturation occurs around 780 K due to minority carrier activation, whereas for the Er-containing sample, a maximum is reached at 860 K (as seen more clearly in the high-temperature data shown in Figure S9). The Goldsmid-Sharp band gap energy (E_g = $2e|S_{max}|T_{max}$) is similar for $PrCuZnP_2$ (0.36 eV) and $NdCuZnP_2$ (0.38 eV), but much lower for $ErCuZnP_2$ (0.23 eV), contradicting the trend in computed band

gaps. This disagreement likely arises because the Goldsmid-Sharp approximation breaks down for highly degenerate samples,[42] as is the case here. Nevertheless, the computed and experimental Seebeck coefficients agree well with each other in terms of magnitude and temperature dependence.

The density of states effective mass m_{DOS}* was estimated from the experimental Seebeck coefficients using the single parabolic band (SPB) model[52] and the three scattering mechanisms (IMP, ADP, POP) proposed above, as shown in Figure S9. The selected type of scattering affects the magnitude of the estimated value of m_{DOS}*, but not the predicted dependence of S on n_H (Figure S10 (b)). Regardless of scattering mechanism, m_{DOS}* increases with higher temperature, indicating a greater number of valence bands or flatter band dispersion (Figure S8). Furthermore, m_{DOS}* is virtually independent of the *RE* component. A similar observation was noted in AZn_2Sb_2 compounds, for which substitution of the divalent *A* component has no effect on m_{DOS}*;[53] these previous reports made use of an SPB model with transport assumed to be limited by acoustic phonon scattering. If the same assumption is applied to the present compounds containing trivalent cations, the m_{DOS}* values (0.9 m_e at 373 K and 1.1 m_e at 673 K) are significantly higher than the average reported in other *p*-type $CaAl_2Si_2$-type compounds (0.6 m_e).[26,33,53] If, instead, the dominant mechanism in *RE*$CuZnP_2$ is assumed to be polar optical scattering, as suggested by the AMSET results above, then the m_{DOS}* values become comparable to those of other *p*-type $CaAl_2Si_2$-type compounds, assuming that they are dominated by acoustic phonon scattering.

Thermal Transport Properties

The total thermal conductivity, which consists of electronic and phononic contributions, $\kappa = \kappa_{el}+\kappa_{ph}$, was measured for *RE*$CuZnP_2$ compounds. The electronic thermal conductivity κ_{el} was estimated from the Wiedemann-Franz law, $\kappa_{el} = L_{eff}(T/\rho)$, and the lattice thermal conductivity κ_{ph} was obtained by subtracting κ_{el} from κ. The effective Lorenz number L_{eff} can be calculated from the SPB model, but it is important to note that the choice of scattering mechanism directly affects L_{eff}, and thus κ_{ph} (see Supporting Information for details and Figure S11 for comparison of various assumptions of scattering type). Because polar optical phonon scattering was shown above to be the most important, it was chosen to calculate L_{eff}. The total thermal conductivity κ of $ErCuZnP_2$ is nearly twice that of $NdCuZnP_2$ and $PrCuZnP_2$ (Figure 3 (a)), mainly because it has a larger electronic contribution. The lattice thermal conductivities κ_{ph} of these compounds are remarkably low (Figure 3 (b)), comparable to that of previously reported $YbCuZnP_2$.[26] As the temperature increases, the values of κ_{ph} decrease due to Umklapp scattering, and at high temperatures, they approach the so-called "glassy limit," which is roughly 0.9 W m^{-1} K^{-1} based on the experimental speed of sound for $ErCuZnP_2$. Given their high speeds of sound, the low κ_{ph} values for *RE*$CuZnP_2$ compounds are rather unexpected. Table 2 shows that these κ_{ph} values are comparable to those of compounds having 30% lower speeds of sound (e.g., $EuZn_2P_2$,[54] $CaMg_2Bi_2$[55]).

To shed light on the relative influence of phonon velocity and relaxation time on κ_{ph}, DFT calculations using compressive sensing lattice dynamics (CSLD)[29] were performed to determine the phonon band structure (Figure 3 (c)). The phonon DOS curve reveals that the acoustic and low-frequency optical modes are dominated by *RE*, Cu, and Zn atoms, whereas the high-frequency modes are dominated by the lighter P atoms. Examining the phonon dispersion curves shows that $ErCuZnP_2$ has the highest group velocity, but it also exhibits stronger anharmonicity, as indicated by the higher mode-averaged Grüneisen parameter of 1.73 (compared to 1.47 for $NdCuZnP_2$). The Grüneisen parameters are slightly lower than that of Mg_3Sb_2 and lie within the range of $CaAl_2Si_2$-type and other Zintl compounds.[34,55,58,60,61] Given its higher anharmonicity, $ErCuZnP_2$ is predicted to have lower κ_{ph} than $NdCuZnP_2$ (Figure 3 (d)). This prediction contradicts the experimental trend in κ_{ph}. The computed κ_{ph} value for $ErCuZnP_2$ is lower than the experimental value, which is surprising given that grain boundaries are not considered in the calculation. It is possible that our "experimental" κ_{ph} values are slightly overestimated due to an underestimate of L_{eff} and thus κ_e. Even if L_{eff} is similarly overestimated for all three compounds, the impact on the "experimental" κ_{ph} for $ErCuZnP_2$ would be the greatest, because it has an order of magnitude higher electrical conductivity than the Pr- or Nd- analogues.

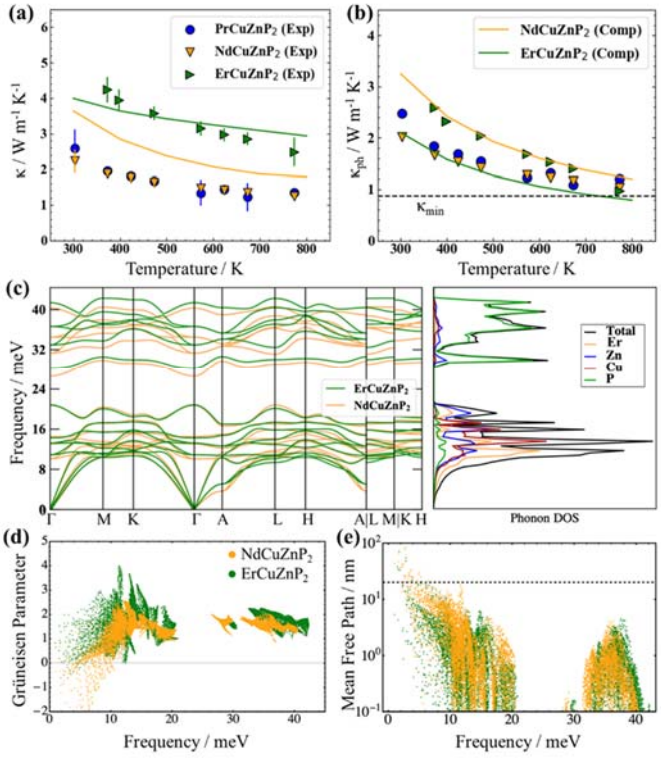

Figure 3. (a) Experimental (symbols) and computed (solid lines) total thermal conductivities and (b) lattice thermal conductivities of *RE*$CuZnP_2$ compounds. (c) Phonon dispersion and DOS curves reveal stiffer phonons in $ErCuZnP_2$ than in $NdCuZnP_2$. (d) Computed mode Grüneisen parameters and (e) phonon mean free paths indicate stronger anharmonicity and smaller average mean free path in $ErCuZnP_2$ than in $NdCuZnP_2$. (Dashed line indicates the grain size limiting the thermal conductivity in $NdCuZnP_2$.) Note that the calculation for $PrCuZnP_2$ did not converge; see Supporting Information for details.

In contrast, the computed κ_{ph} value for $NdCuZnP_2$ is overestimated relative to the experimental value, the

discrepancy potentially arising from impurities, grain boundaries, or point defect scattering (e.g., Cu/Zn disorder, notwithstanding the small mass contrast) which are not included in the calculations. To gauge the effects of grain boundary scattering, the lattice thermal conductivity was also calculated as a function of mean free path (Figure S13). Grain sizes of 25±5 nm in $NdCuZnP_2$ would scatter the majority of acoustic phonons (above the dashed line shown in Figure 3 (e)), reproducing the experimental κ_{ph} value. The thermal conductivity was computed by combining the lattice thermal conductivity derived from lattice dynamics (Figure 3 (b)) and the electronic thermal conductivity derived from electron scattering calculations. In general, the computed and experimental thermal conductivities agree reasonably (Figure 3 (a)).

Thermoelectric Figure of Merit

The electrical and thermal transport properties were combined to evaluate the experimental and computed thermoelectric figures of merit *zT* (Figure 4). The experimental figure of merit rises to nearly 0.5 at 780 K for $ErCuZnP_2$ and $NdCuZnP_2$, with the trend suggesting further increase at higher temperature, and reaches a maximum of 0.3 at 773 K for $PrCuZnP_2$. These values are nearly comparable to previously reported *zT* of $YbCuZnP_2$, which reaches a peak *zT* of 0.6 at 1000 K.[26] Given the temperature dependence, it is likely that the performance of the present compounds will surpass $YbCuZnP_2$, ranking them among the best phosphide thermoelectrics yet.[19,26] The experimental and computed figures of merit agree reasonably well with each other, particularly for $ErCuZnP_2$. The small discrepancies can be traced mainly to the neglect of the imperfect crystallinity of the samples, e.g., grain boundary and disorder scattering in the calculation of hole mobilities. When grain boundary scattering is included in $PrCuZnP_2$ and $NdCuZnP_2$, the computed electronic and thermal properties are slightly closer to experiment, but there is only a minor effect on *zT* (see details in Supporting Information and Figure S14).

The thermoelectric measurements were made on unoptimized samples, meaning that there is room for improvement. Because the thermoelectric figure of merit *zT* is strongly related to carrier concentration n_H, this dependence was examined in more detail at 673 K (Figure S12). When the AMSET model was applied, the results suggest that the figure of merit for $ErCuZnP_2$ can be significantly improved by doping to achieve a carrier concentration to about $5 \cdot 10^{19}$ cm^{-3} or potentially by using single-crystal samples. A similar trend of *zT* vs n_H was obtained when the SPB model was applied. Assuming polar optical phonon scattering vs. acoustic phonon scattering leads to major differences in the dependence of mobility and L_{eff} on carrier concentration and chemical potential, and thereby the figure of merit (Figure S10 (a), S11, and S12 (a)). In particular, the mobility is nearly independent of carrier concentration under polar optical phonon scattering, consistent with the relatively carrier-independent mobility in $CaAl_2Si_2$-type compounds. This leads to a prediction of a higher optimum carrier concentration if the predictions from AMSET are correct, and polar optical phonon scattering is dominant in this system.

Table 2. Theoretical density (in g cm^{-3}), computed average speed of sound (v_{avg} in m s^{-1}), computed mode-averaged Grüneisen parameter, and experimental minimum lattice thermal conductivity ($\kappa_{ph,exp}$ in W m^{-1} K^{-1}) of selected $CaAl_2Si_2$-type compounds. The speed of sound is calculated from computed elastic properties from Table 1 and MaterialsProject.org.[56]

Compound	Density	v_{avg}	Grüneisen parameter	$\kappa_{ph,exp}$	Ref.
$PrCuZnP_2$	5.70	3,900		1.1	This work
$NdCuZnP_2$	5.82	3,880	1.5	1.0	This work
$ErCuZnP_2$	6.67	3,680	1.7	1.0	This work
$YbCuZnP_2$	6.64			0.9-1.0	26
$CaZn_2P_2$	3.93	4,190		1.0	26
$CaMg_2Sb_2$	3.87	3,210	1.4	1.6	34, 57
Mg_3Sb_2	4.04	2,790	1.8; 1.8–2.2	0.6	34, 58, 59
$CaMg_2Bi_2$	5.66	2,480	1.5	1.2	55
$CaZn_2Sb_2$	5.40	2,480	1.8	1.9	60
$EuZn_2Sb_2$	6.78	2,400		1.1	54
$CaCd_2Sb_2$	5.95	2,380	1.7	0.7	61, 62
$SrZn_2Sb_2$	5.68	2,320		1.2	63
$YbMn_2Sb_2$	6.71	2,070		2.2	64

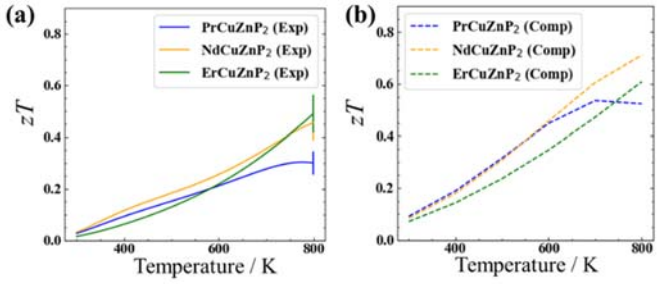

Figure 4. (a) Experimental and (b) computed thermoelectric figure of merit as a function of temperature for *RE*$CuZnP_2$. The computed *zT* was obtained using the electronic properties (AMSET) and the lattice thermal conductivity (CSLD). Note that κ_{ph} for $PrCuZnP_2$ was set to the one for $NdCuZnP_2$.

Conclusions

Based on a high-throughput screening of >20,000 compounds, the phosphides *RE*$CuZnP_2$ (*RE* = Pr, Nd, Er) were predicted to be promising thermoelectric materials that are unconventional candidates because lightweight compounds are not normally considered. These predictions were validated by experimental measurements, which indicated that their thermoelectric

performance is promising even before optimization by appropriate doping. First-principles calculations coupled with advanced scattering models of electronic and phononic properties successfully modelled the experimental transport of these compounds, notwithstanding their complex crystal structures. The hole transport in these compounds is predicted to be mostly limited by polar optical phonon scattering, suggesting that polar optical phonon scattering may be more widespread than previously thought, which has important consequences for strategies used to optimize the thermoelectric figure of merit. The lattice thermal conductivities of *RE*$CuZnP_2$ compounds are quite low, despite their stiff elastic moduli and high speeds of sound. In particular, for $ErCuZnP_2$, strong anharmonicity may be responsible for low κ_{ph} values that approach the glassy limit (about 1 W m^{-1} K^{-1}). This study is a promising indicator that AMSET and CSLD are sufficiently robust to screen the thermoelectric properties of complex materials that have been traditionally avoided in high throughput studies. This methodology of using first-principles calculations to identify and explore electron/hole scattering can be extended generally and has implication to all classes of thermoelectric and other functional materials.

Conflicts of interest

There are no conflicts to declare.

Notes and references

Supporting information is available from the journal or from the author.

Acknowledgments

This work was supported by the Canada First Research Excellence Fund (CFREF, through the Future Energy Systems Research Institute at the University of Alberta, Project T12-P01) and the Natural Sciences and Engineering Research Council of Canada (NSERC, through Discovery Grant RGPIN-2018-04294). JHP acknowledges the FRQNT PBEEE postdoctoral fellowship. This work was supported by the NASA Science Missions Directorate under the Radioisotope Power Systems Program's Thermoelectric Technology Development Project. Synthesis-related tasks performed by SC and AZ were supported by the National Science Foundation (NSF) award number 1709158. SC's contributions are based upon work supported by the National Science Foundation Graduate Research Fellowship Program award number DGE-1848739. Computational efforts by JP, AG, AD, and AJ were funded by the U.S. Department of Energy (DOE), Office of Basic Energy Sciences, Early Career Research Program. This research used resources of the National Energy Research Scientific Computing Center, which is supported by the Office of Science of the U.S. Department of Energy under Contract No. DEAC02-05CH11231. Lawrence Berkeley National Laboratory is funded by the DOE under award DE-AC02-05CH11231.

1 G. J. Snyder and E. S. Toberer, *Nat. Mater.,* 2008, **7**, 105.
2 P. Gorai, E. S. Toberer, and V. Stevanovic, *Phys. Chem. Chem. Phys.*, 2016, **18**, 31777.
3 L. Bjerg, G. K. H. Madsen, and B. B. Iversen, *Chem. Mater.,* 2011, **23**, 3907.
4 G. K. H. Madsen, *J. Amer. Chem. Soc.,* 2006, **128**, 12141.
5 J. He, M. Amsler, Y. Xia, S. S. Naghavi, V. I. Hegde, S. Hao, S. Goedecker, V. Ozoliņš, and C. Wolverton, *Phys. Rev. Lett.,* 2016, **177**, 046602.
6 J. Carrete, N. Mingo, S. Wang, and S. Curtarolo, *Adv. Funct. Mater.*, 2014, **24**, 7427.
7 H. Zhu, G. Hautier, U. Aydemir, Z.M. Gibbs, G. Li, S. Bajaj, J.-H. Pöhls, D. Broberg, W. Chen, A. Jain, M. A. White, M. Asta, G. J. Snyder, K. Persson, and G. Ceder, *J. Mater. Chem. C*, 2015, **3**, 10554.
8 U. Aydemir, J.-H. Pöhls, H. Zhu, G. Hautier, S. Bajaj, Z. M. Gibbs, W. Chen, G. Li, S. Ohno, D. Broberg, S. D. Kang, M. Asta, G. Ceder, M. A. White, K. Persson, A. Jain, and G. J. Snyder, *J. Mater. Chem. A,* 2016, **4**, 2461.
9 G. Bergerhoff, I. Brown and F. Allen, Crystallographic Databases, International Union of Crystallography, Chester, 1987.
10 H. Tamaki, H. K. Sato, and T. Kanno, *Adv. Mater.,* 2016, **28**, 10182–10187.
11 K. Imasato, S. D. Kang, and G. J. Snyder, *Energy Environ. Sci.,* 2019, **12**, 965-971.
12 X. Shi, T. Zhao, X. Zhang, C. Sun, Z. Chen, S. Lin, W. Li, H. Gu, and Y. Pei, *Adv. Mater.,* 2018, **31**, 1903387.
13 H. Zhang, L. Fang, M.-B. Tang, H.-H. Chen. X.-X. Yang, X. Guo, J.-T. Zhao, and Y. Grin, *Intermetallics*, 2010, **18**, 193.
14 P. E. R. Blanchard, S. S. Stoyko, R. G. Cavell, and A. Mar*, J. Solid State Chem.*, 2011, **184**, 97.
15 A. T. Nientiedt, H. Lincke, U. Ch. Rodewald, R. Pöttgen, and W. Jeitschko, *Z. Naturforsch. B*, 2011, **66b**, 221-226.
16 J. Prakash, M. C. Schäfer, and S. Bobev, *Acta Cryst.,* 2015, **C71**, 894–899.
17 Y. Kumashiro, M. Hirabayashi, T. Koshiro, and Y. Okada, *J. Less-Common Metals,* 1988, **143**, 159–165.
18 J.-H. Pöhls, A. Faghaninia, G. Petretto, U. Aydemir, F. Ricci, G. Li, M. Wood, S. Ohno, G. Hautier, G. J. Snyder, G.-M. Rignanese, A. Jain, and M. A. White, *J. Mater. Chem. C,* 2017, **5**, 2050.
19 J. Nuss, U. Wedig, W. Xie, P. Yordanov, J. Bruin, R. Hübner, A. Weidenkaff, and H. Takagi, *Chem. Mater.,* 2017, **29**, 16, 6956-6965.
20 W.D. Thompson, R. Vaddi, and B.E. White Jr., *J. Alloys Comp.,* 2016, **687**, 813-820.
21 P. Klüfers and A. Mewis, *Z. Naturforsch. B,* 1977, **32**, 753–756.
22 P. Klüfers and A. Mewis, *Z. Naturforsch. B*, 1977, **32**, 353–354.
23 H.-O. Fischer and H.-U. Schuster, *Z. Naturforsch. B*, 1977, **35**, 1322–1323.
24 S. L. Brock, J.E. Greedan, and S. M. Kauzlarich, *J. Solid State Chem.*, 1994, **113**, 303-311.
25 V. Ponnambalam and D. T. Morelli, *J. Electron. Mater.*, 2014, **43**, 1875–1880.
26 V. Ponnambalam, S. Lindsey, W. Xie, D. Thompson, F. Drymiotis, and Terry M. Tritt, *J. Phys. D: Appl. Phys.*, 2011, **44**, 155406.
27 A. C. Payne. A. E. Sprauve, M. M. Olmstead, S. M. Kauzlarich, J. Y. Chan, B. A. Reisner, and J. W. Lynn, *J. Solid State Chem.,* 2002, **163**, 498-505.
28 O. Reckeweg, C. Lind, A. Simon, and F. J. DiSalvo, *Z. Naturforsch. B*, 2002, **58**, 159–162.
29 F. Zhou, W. Nielson, Y. Xia, and V. Ozoliņš, *Phys. Rev. Lett.,* 2014, **113**, 185501.
30 J. J. Kuo, U. Aydemir, J.-H. Pöhls, F. Zhou, G. Yu, A. Faghaninia, F. Ricci, M. A. White, G.-M. Rignanese, G. Hautier, A. Jain, and G. J. Snyder*, J. Mater. Chem. A,* 2019, **7**, 2589.
31 E. S. Toberer, A. Zevalkink, and G. J. Snyder, *J. Mater. Chem.,* 2011, **21**, 15843-15852.

32 A. Ganose, J. Park, A. Faghaninia, R. Woods-Robinson, K. A. Pearsson, and A. Jain, arXiv:2008.09734v1 [cond-mat.mtrl-sci] 22 Aug 2020.
33 W. Peng, S. Chanakiana, and A. Zevalkink, *Inorg. Chem. Front.*, 2018, **5**, 1744-1759.
34 W. Peng, G. Petretto, G.-M. Rignanese, G. Hautier, and A. Zevalkink, *Joule*, 2018, **2**, 1879–1893.
35 S. M. Kauzlarich, C. L. Condron, J. K. Wassei, T. Ikeda, and G. J. Snyder, *J. Solid State Chem.*, 2009, **182**, 240-245.
36 Y. Hinuma, T. Hatakeyama, Y. Kumagai, L. A. Burton, H. Sato, Y. Muraba, S. Iimura, H. Hiramatsu, I. Tanaka, H. Hosono, and F. Oba, *Nature Commun.*, 2016, **7**, 11962.
37 G. S. Pomrehn, A. Zevalkink, W. G. Zeier, A. van de Walle, and G. J. Snyder, *Angew. Chem. Int. Ed.*, 2014, **53**, 3422-3426.
38 H. Zhang, J.-T. Zhao, Y. Grin, X.-J. Wang, M.-B. Tang, Z.-Y. Man, H.-H. Chen, and X.-X. Yang, *J. Chem. Phys.*, 2008, **129**, 164713.
39 F. Gascoin, S. Ottensmann, D. Stark, S. M. Haile, and G. J. Snyder, *Adv. Funct. Mater.*, 2005, **15**, 1860.
40 A. F. May, M. A. McGuire, D. J. Singh, J. Ma, O. Delaire, A. Huq, W. Cai, and H. Wang, *Phys. Rev. B,* 2012, **85**, 035202.
41 J. Heyd, G. E. Scuseria, and M. Ernzerhof, *J. Chem. Phys.*, 2003, **118**, 8207.
42 Z. M. Gibbs, F. Ricci, G. Li, H. Zhu, K. Persson, G. Ceder, G. Hautier, A. Jain, and G. J. Snyder, *npj Comput. Mater.*, 2017, **32**, 8.
43 F. Ricci, W. Chen, U. Aydemir, G. J. Snyder, G.-M. Rignanese, A. Jain, and G. Hautier, *Sci. Data*, 2017, **4**, 170085.
44 J. Zhang, L. Song, and B. B. Iversen, *npj Comput. Mater.*, 2019, **5**, 76.
45 J. Noffsinger, F. Giustino, B. D. Malone, C.-H. Park, S. G. Louie, and M. L. Cohen, *Comput. Phys. Commun.*, 2010, **181**, 2140-2148.
46 S. Poncé, W. Li, S. Reichardt, and F. Giustino, *Rep. Prog. Phys.,* 2020, **83**, 036501.
47 Y. Pei, H. Wang, and G. J. Snyder, *Adv. Mater.*, 2012, **24**, 6125-6135.
48 J. Cao, J. D. Querales-Flores, A. R. Murphy, S. Fahy, and I. Savić, *Phys. Rev. B*, 2018, **98**, 205202.
49 J. Ma, Y. Chen, and W. Li, *Phys. Rev. B*, 2018, **97**, 205207.
50 J. Zhou, H. Zhu, T.-H. Liu, Q. Song, R. He, J. Mao, Z. Liu, W. Ren, B. Liao, D. J. Singh, Z. Ren, and G. Chen, *Nat. Commun.*, 2018, **9**, 1721.
51 J. Park, Y. Xia, and V. Ozoliņš, *Phys. Rev. Appl.*, 2019, **11**, 014058.
52 A. F. May, E. S. Toberer, A. Saramat, and G. J. Snyder, *Phys. Rev. B: Condens. Matter Mater. Phys.*, 2009, **80**, 125205.
53 E. S. Toberer, A. F. May, B. C. Melot, E. Flage-Larsen, and G. J. Snyder, *Dalton Trans.*, 2010, **39**, 1046.
54 Y. Takagiwa, Y. Sato, A. Zevalkink, I. Kanazawa, K. Kimura, Y. Isoda, and Y. Shinohara, *J. Alloys Compd.*, 2017, **703**, 73-79.
55 C. Sun, X. Shi, L. Zheng, B. Chen, and W. Li, *J. Materiomics,* 2019, **5**, 567-573.
56 M. de Jong, W. Chen, T. Angsten, A. Jain, R. Notestine, A. Gamst, M. Sluiter, C. K. Ande, S. Van Der Zwaag, J. J. Plata, C. Toher, S. Curtarolo, G. Ceder, K. A. Persson, and M. Asta, *Sci. Data*, 2015, **2**, 150009.
57 M. Wood, U. Aydemir, S. Ohno, and G.J. Snyder, *J. Mater. Chem. A,* 2018, **6**, 9437-9444.
58 J. Zhang, L. Song, M. Sist, K. Tolborg, and B. B. Iversen, *Nat. Commun.,* 2018, **9**, 4716.
59 Z. Ren, J. Shuai, J. Mao, Q. Zhu, S. Song, Y. Ni, and S. Chen, *Acta Mater.*, 2018, **143**, 265-271.
60 T.A. Wubieneh, P.C. Wei, C.C. Yeh, S. Chen, and Y.-Y. Chen, *J. Electron. Mater.*, 2016, **45**, 1942–1946.
61 T. Pandeya and A. K. Singh, *Phys. Chem. Chem. Phys.*, 2015, **17**, 16917-16926.
62 Q.-G. Cao, H. Zhang, M.-B. Tang, H.-H. Chen, X.-X. Yang, Y. Grin, and J.-T. Zhao, *J. Appl. Phys.*, 2010, **107**, 053714.
63 H. Zhang, M.-B. Tang, W. Schnelle, M. Baitinger, Z.-Y. Man, H.-H. Chen, X.-X. Yang, J.-T. Zhao, and Y. Grin, *J. Electron Mater.*, 2010, **39**, 1772-1776.
64 K. Guo, Q-G. Cao, X.-J. Feng, M.-B. Tang, H.-H. Chen, X. Guo, L. Chen, Y. Grin, and J.-T. Zhao, *Eur. J. Inorg. Chem.*, 2011, **2011**, 4043–4048.